PHYSICAL REVIEW E **107**, 034801 (2023)

Surface diffusion in narrow channels on curved domains

Aldo Ledesma-Durán,[1,*] D. Assaely León-Velasco,[2,†] Guillermo Chacón-Acosta,[2,3,‡] and L. Héctor Juárez-Valencia[1,§]
[1]*Departamento de Matemáticas, Universidad Autónoma Metropolitana Iztapalapa, Iztapalapa, Vicentina, 09340 Ciudad de México, Mexico*
[2]*Departamento de Matemáticas Aplicadas y Sistemas, Universidad Autónoma Metropolitana Cuajimalpa, 05348 Ciudad de México, Mexico*
[3]*Institute of Physics and Astronomy, University of Potsdam, 14476 Potsdam-Golm, Germany*

(Received 15 December 2022; accepted 15 February 2023; published 2 March 2023)

We study the transport properties of diffusing particles restricted to confined regions on curved surfaces. We relate particle mobility to the curvature of the surface where they diffuse and the constraint due to confinement. Applying the Fick-Jacobs procedure to diffusion in curved manifolds shows that the local diffusion coefficient is related to average geometric quantities such as constriction and tortuosity. Macroscopic experiments can record such quantities through an average surface diffusion coefficient. We test the accuracy of our theoretical predictions of the effective diffusion coefficient through finite-element numerical solutions of the Laplace-Beltrami diffusion equation. We discuss how this work contributes to understanding the link between particle trajectories and the mean-square displacement.

DOI: 10.1103/PhysRevE.107.034801

I. INTRODUCTION

Surface diffusion is the process of particle migration in the adsorbed state. This process generally increases mass transfer rates since adsorbed particles can migrate along the surface, producing a new flux besides that of bulk transport [1–5]. It is believed that surface diffusion is responsible for most of the mass transport of some fluids through porous media in some materials [6,7].

Nowadays, several experimental techniques deal with the influence of surface diffusion in chemical reactors [8–15]. Those experiments show that temperature and fractional coverage generally increase the surface diffusion coefficient. However, in such measurements, the differences between mass and surface fluxes are often not well defined since the results differ depending on the model or experiment used [6]. The problem is partly due to the lack of an appropriate definition of an effective diffusion coefficient that can relate the mesoscopic-level Fick diffusion laws, valid locally in each surface region, with the experimentally measured macroscopic flux at the reactor ends [16,17]. This should reflect how the irregular structure of the trajectories, due to the decrease in available surface area (characterized, for example, by its concavity, tortuosity, and degree of constriction) affects the reactor-scale flow; therefore, it should capture the differences with the transport over a perfectly flat unbounded surface where a diffusion coefficient of D_0 is measured [18–20].

In this work, we study the relationship between the local surface diffusion coefficient D_0 with a surface diffusion coefficient D^* that would be obtained on a surface where the restriction in the trajectories reduces the mean-square displacement (MSD) of the adsorbed particles. To understand the distinction between the two coefficients, we can consider their differences in analogy to bulk transport in the reactor. For volumetric diffusion occurring within a porous medium, we know that the effective diffusion coefficient D_b^* (i.e., the one that measures the relation between flux and concentration difference at the two ends of the reactor) is reduced compared to the molecular diffusion coefficient D_b due to the reduction of the available space. The influence of the solid matrix in this reduction can be classified as follows: (1) the empty or available space is reduced, (2) the particles do not travel in a straight line but in winding paths through the pores, and (3) the pore openings and bottlenecks change the local velocity of the fluid. The mathematical form of these three coefficients was recently obtained using the so-called Fick-Jacobs approach [21] and proved efficient for describing bulk flow in experiments and numerical simulations over a range of regimes [22–24].

We will show that similar ideas of entropic constraints applied to curved manifolds lead to similar expressions for reducing the diffusion coefficient by redefining these three factors in terms of surface-related geometric quantities. Therefore, our approach allows us to model cases of surface diffusion under confinement due to barriers or obstacles as it occurs in many examples [25–27]. This leads to an expression for the effective surface diffusion coefficient D^* close to that of Lifson-Jackson in Refs. [28,29].

For this purpose, we will determine how the spatial configuration of the boundaries on a confined surface affects the effective particle displacement along the spatial coordinate determined by the characteristic direction of the reactor. The Fick-Jacobs (FJ) approach allows linking the pores' local geometric structure with a longitudinal effective diffusion coefficient that explicitly incorporates the shape of the available domain boundary [21,30,31]. This approximation has been

---

[*] aldo_ledesma@xanum.uam.mx
[†] dleon@cua.uam.mx
[‡] gchacon@cua.uam.mx
[§] hect@xanum.uam.mx

used to study bulk diffusion in confined media such as pores and channel-like regions, where one coordinate is considerably larger than the other. Under this assumption, it is possible to obtain an effective diffusion equation along just the longitudinal direction, containing a diffusion coefficient $D_{\mathrm{FJ}}(x)$ that depends on the channel geometry and serves as a bridge to link the former two diffusion coefficients [32,33]. There are different methods to obtain this position-dependent diffusion coefficient under various circumstances. The Kalinay-Percus method is a rigorous projection method based on series inversion that has been applied for symmetric and asymmetric channels in two or three dimensions [34–37]. Through a geometrical method that describes the channel boundaries from the reference system of its centerline, it is also possible to approximately get this kind of spatial-dependent coefficient for channels with nonzero curvature and torsion midlines [38–40]. Using a similar approach, we study surface diffusion in constrained domains. Just as solid pores in the solid matrix of a porous material constitute a constraint to mass diffusion, we show that constrained regions can be modeled as a patch that restricts the available surface area and, consequently, the surface diffusion coefficient measured through MSD measurements.

The organization of work is as follows. In Sec. II A, we use Fick's diffusion equation on parametric surfaces using the Laplace-Beltrami operator in the diffusion equation to include the metric of the surface. Then, to unravel the role of geometrical constraints set by surface boundaries, in Sec. II B, we use the Fick-Jacobs projection approach, which explicitly incorporates the patch geometry into a local diffusion coefficient. In Sec. II C, we will then explain how local properties of surface geometry can be averaged in terms of more general and intuitive parameters commonly used to describe macroscopic porous media, such as tortuosity and constriction of the trajectories. In Sec. III, we corroborate our theoretical predictions with numerical simulations using a finite-element approximation of the Laplace-Beltrami diffusion equation [41] for various pores in different regular surfaces and discuss how these approximations are reflected in macroscopic flux measurements of MSD. Finally, Sec. IV is dedicated to discussing our conclusions.

II. THEORETICAL APPROACHES TO THE DIFFUSION ON A SURFACES

A. Surface diffusion using the Laplace-Beltrami operator

The diffusion equation for the concentration of particles on a surface is $\frac{\partial C}{\partial t} = D_0 \nabla_s^2 C$, where ∇_s^2 is the Laplace-Beltrami operator. In this equation, D_0 is the surface diffusion coefficient that measures the ratio between the local concentration gradient and the flux along the surface, and C is the surface concentration of particles [42]. This equation assumes no interaction among particles and that the only influence of the surface on the particles is to attach them to it. The diffusion coefficient D_0 measures the local displacements and, hence, is independent of the boundaries or curvature of the surface; besides, assuming low coverage, pressure, and temperature, it can be considered constant.

The surface where diffusion occurs is parameterized with $\mathbf{X} = (x(\xi,\eta), y(\xi,\eta), z(\xi,\eta))$, where ξ and η are the local coordinates. If such a surface is regular (like the spheres and cylinders of revolution we consider in this work), then the tangent vectors to each coordinate define the metric components, namely $g_{\xi\xi} = X_\xi^2 = |\mathbf{X}_\xi|^2$, $g_{\eta\eta} = X_\eta^2 = |\mathbf{X}_\eta|^2$, and $g_{\xi\eta} = g_{\eta\xi} = \mathbf{X}_\xi \cdot \mathbf{X}_\eta = 0$. Although the regularity requirement for the parametrization may seem very restrictive, many surfaces admit coordinates with zero off-diagonal metric components. For these coordinates, the diffusion equation for the surface concentration $C(\xi,\eta,t)$ reduces to

$$\frac{\partial C}{\partial t} = \frac{D_0}{\sqrt{g_{\xi\xi} g_{\eta\eta}}} \left\{ \frac{\partial}{\partial \xi}\left[\sqrt{\frac{g_{\eta\eta}}{g_{\xi\xi}}}\frac{\partial C}{\partial \xi}\right] + \frac{\partial}{\partial \eta}\left[\sqrt{\frac{g_{\xi\xi}}{g_{\eta\eta}}}\frac{\partial C}{\partial \eta}\right]\right\}, \quad (1)$$

where g_{ab} are the components of the metric tensor. This equation quantifies how the local domain metric influences the diffusion of particles compared to the case of a planar surface where $g_{\xi\xi} = g_{\eta\eta} = 1$ and $g_{\xi\eta} = 0$. If the metric does not depend on one of the coordinates, say, on η, then the above equation simplifies to

$$\frac{\partial C}{\partial t} = \frac{D_0}{X_\xi X_\eta} \left\{ \frac{\partial}{\partial \xi}\left[\frac{X_\eta}{X_\xi}\frac{\partial C}{\partial \xi}\right] + \frac{X_\xi}{X_\eta}\left(\frac{\partial^2 C}{\partial \eta^2}\right)\right\}. \quad (2)$$

This equation describes the evolution of the concentration and, using appropriate boundary conditions, can be solved on confined surfaces. However, this form of diffusion equation does not explicitly establish how the domain geometry affects the transport. Such effects will be studied from two different perspectives in the following subsections.

B. Confined surface diffusion using the Fick-Jacobs approximation

Consider that the adsorbed particles do not move over an infinite region (such as an infinite cylinder) or a closed surface (such as a sphere or a torus) but over a subset bounded by physical or chemical boundaries. Additionally, let us assume that this diffusion domain consists of an elongated zone where the direction defined by the local ξ coordinate is much longer than the other.

We can then identify the irregular form of our domain as that formed by the points $(\xi,\eta) \in \Omega_0 = [\xi_i, \xi_f] \times [\eta_1(\xi), \eta_2(\xi)]$, where $\eta_1(\xi)$ and $\eta_2(\xi)$ are the long boundaries whose irregular shape changes with ξ, see Fig. 1(a). We will assume that zero flux conditions in these two boundaries confine the trajectories; therefore, there is no material entry through the patch's lateral walls.

In this situation, where one of the characteristic dimensions of the patch is larger than the other, we can assume that the concentration equilibrates at a slower rate in the longitudinal direction ξ. Then, it is possible to average the diffusion equation in (1) in the shorter direction η using the FJ procedure [30]. By this, we obtain an equation for the marginal surface concentration $c(\xi,t)$ yielding the following:

$$X_\xi X_\eta \frac{\partial c}{\partial t} = \frac{\partial}{\partial \xi}\left[D_s w(\xi)\frac{X_\eta}{X_\xi}\frac{\partial}{\partial \xi}\left(\frac{c}{w}\right)\right]. \quad (3)$$

The function $w(\xi) \equiv \eta_2(\xi) - \eta_1(\xi)$ is the local width of the patch and $y(\xi) = [\eta_1(\xi) + \eta_2(\xi)]/2$ describes its midline. These two geometrical quantities are sketched in Fig. 1(a) and

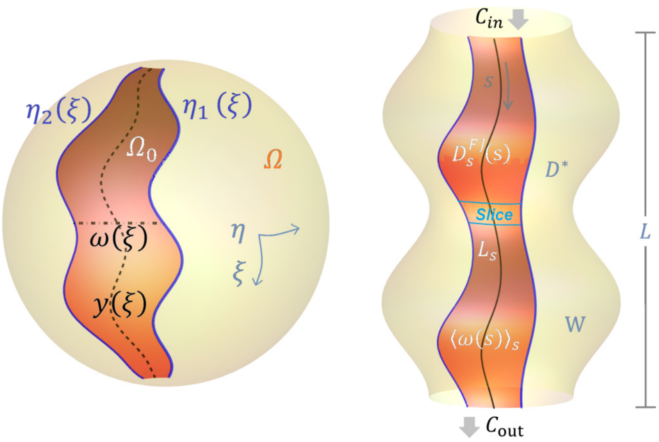

FIG. 1. Representative patch in a sphere. (a) Parameters in the Fick-Jacobs description of surface diffusion. (b) Parameters in the macroscopic description of surface diffusion.

determine the influence of the confinement in the description of the diffusion. The relation between the joint concentration C in Eq. (2) and the marginal concentration c in (3) is

$$c(\xi,t)=\int_{\eta_1(\xi)}^{\eta_2(\xi)}C(\xi,\eta,t)d\eta. \tag{4}$$

When D_s in Eq. (3) is taken directly to be D_0, we have the zero-order approximation of (1) and the FJ procedure has the advantage of including the form of the lateral boundaries explicitly in the equation on the term $w(\xi)$. However, obtaining higher-order approximation terms in the description of longitudinal transport is possible using recursive methodologies. In this case, Eq. (3) is adjusted to include the geometric features of the patch through a coordinate-dependent diffusion coefficient FJ, $D_s\to D_s^{\text{FJ}}(\xi)$. For example, using the Kalinay-Percus scheme [30,31], the Fick-Jacobs diffusion coefficient D_s^{FJ} in first-order approximation is

$$D_s^{\text{FJ}}(\xi)\approx D_0\left\{1+\frac{X_\eta^2}{X_\xi^2}\left[y'^2(\xi)+\frac{1}{12}w'^2(\xi)\right]\right\}^{-1}. \tag{5}$$

It accounts for how the constriction of the stripped patch, measured by $w'^2(\xi)$, and its tortuosity, measured by $y'^2(\xi)$, cause a reduction in the motion of particles along the main direction of transport.

The solution of the FJ equation (3) using the diffusion coefficient (5) has been tested against numerical simulations of the original transport equation (2) using finite-element and Brownian motion simulations in planar surfaces with successful results [16,17,43–45]. This justifies its use as a link between the molecular and macroscopic diffusion coefficients.

C. Effective surface diffusion coefficient in long reactors

Now consider the case where surface diffusion occurs in a large reactor. The particles do not necessarily occupy the entire internal surface or travel along the shortest surface path. These entropic restrictions limit the motility of the particles by lowering the measured diffusion coefficient. However, measuring this reduction by solving the diffusion equation for each internal patch covered by the trajectories is not practical. It is, therefore, necessary to obtain an effective diffusion coefficient, D^*, that measures the proportionality between the inlet and outlet flows and the concentration differences at both ends of the reactor. For this procedure to be practical, this coefficient should not refer to the internal detail of the actual trajectories used by the particles but only consider the reduction of the diffusive flux through average quantities. To estimate this decrease, we will compare the reduced flow rate due to the confinement of the trajectories, deduced from the Fick-Jacobs approach, with a macroscopic flux that only considers the length of the reactor and the concentration difference between its outermost boundaries.

For estimating the local flux within the patch from the Fick-Jacobs approach, we can reformulate Eq. (3) as a function defined on the coordinates measured from the midline, i.e., as a function of its arc length s:

$$s(\xi)=\int_{\xi_i}^{\xi}\gamma(\xi')X_\xi(\xi')d\xi', \tag{6}$$

where the scale factor

$$\gamma(\xi)=\sqrt{1+\frac{X_\eta^2}{X_\xi^2}\left(\frac{dy}{d\xi'}\right)^2}, \tag{7}$$

measures the change in length of the trajectories due to the tortuosity of the midline. The interval of this coordinate starts at the input position of the reactor at $s(\xi_i)=0$ and ends at its output position at $s(\xi_f)=L_s$. Note that the midline coincides with a geodesic of the surface for symmetric channels, and the square root in the above expression becomes 1. By taking the arc length s as the transport coordinate, Eq. (3) becomes

$$\frac{\partial c(s,t)}{\partial t}=\frac{\gamma(s)}{X_\eta(s)}\frac{\partial}{\partial s}\left[D_s^{\text{FJ}}(s)w(s)X_\eta(s)\gamma(s)\frac{\partial}{\partial s}\frac{c(s,t)}{w(s)}\right]. \tag{8}$$

This expression is similar to the one obtained in Ref. [38], where the channel is built from its midline, from where the diffusion is described. The surface effect is encoded in the additional factor X_η, which equals 1 for the flat case. In fact, s and ξ are proportional to each other for the specific situation of using polar geodesic coordinates [46]. In Eq. (8), the longitudinal coordinate has been replaced by the arc length (6) in all the related functions since we will assume that the arc length s is a one-to-one function of ξ or, in geometrical terms, that the middle line has no loops and no returns.

To compare with the macroscopic flux, from Eq. (8) we define the averaged longitudinal concentration as:

$$\mathcal{C}(\xi,t)\equiv\frac{c(\xi,t)}{w(\xi,t)}=\frac{1}{\eta_2(\xi)-\eta_1(\xi)}\int_{\eta_1(\xi)}^{\eta_2(\xi)}C(\xi,\eta,t)d\eta. \tag{9}$$

This concentration has the same units as C and, as its mathematical structure suggests, it reflects the longitudinal concentration when variations in the transverse coordinate are averaged. Indeed, it reduces to the joint concentration when the latter does not depend on the transverse coordinate. By defining the pore width as $\omega(s)=w(s)X_\eta(s)$, we can rewrite the Fick-Jacobs equation in (8) as

$$\frac{\omega(s)}{\gamma(s)}\frac{\partial \mathcal{C}}{\partial t}=\frac{\partial}{\partial s}\left[D_s^{\mathrm{FJ}}(s)\omega(s)\gamma(s)\frac{\partial \mathcal{C}}{\partial s}\right]. \qquad (10)$$

From this equation, it is clear that the stationary flow along the midline coordinate, $H(s)$, is achieved when

$$H(s)=-D_s^{\mathrm{FJ}}(s)\omega(s)\gamma(s)\frac{\partial \mathcal{C}}{\partial s} \qquad (11)$$

is constant. This flux $H(s)$ represents the number of particles traveling along the arc length s; in this sense, it is local (depends on s). To consider the flux throughout the entire patch, from $s=0$ to $s=L_s$, we can follow the procedure for a flat surface described in Ref. [21]. Consider a local concentration difference over a distance segment of arc length Δs, i.e., $\Delta\mathcal{C}_s=\mathcal{C}(s+\Delta s)-\mathcal{C}(s)$. The particle flux along this segment can be estimated from (11) as

$$H(s)=-D_s^{\mathrm{FJ}}(\hat{s})\omega(\hat{s})\gamma(\hat{s})\frac{\Delta\mathcal{C}_s}{\Delta s}, \qquad (12)$$

where $\hat{s}$ is a point between s and $s+\Delta s$. The inverse of the factor that multiplies $\Delta\mathcal{C}_s$ is the flow resistance due to that segment. Therefore, considering the resistance to flow of the entire domain as the sum of all the resistances in parallel, the flow between both ends of the reactor, with external concentrations $\mathcal{C}(s=0)=C_{\text{in}}$ and $\mathcal{C}(s=L_s)=C_{\text{out}}$, is

$$H=-\Delta C\left[\int_0^{L_s}\frac{ds}{D_s^{\mathrm{FJ}}(s)\omega(s)\gamma(s)}\right]^{-1}. \qquad (13)$$

Here $\Delta C=C_{\text{out}}-C_{\text{in}}$ is the concentration difference at both ends of the reactor, see Fig. 1(b).

Now let us compare this flow with the one obtained by assuming that the patch is the inside of a large reactor of which we only know its end-to-end length, L_ξ, and its total internal surface area $A_{\text{tot}}=WL_\xi$. In this definition, W is a characteristic width of the entire surface along the cross-sectional coordinate. The confined region $\mathcal{S}_0=\{\mathbf{X}(\xi,\eta)\in\mathbb{R}^3|(\xi,\eta)\in\Omega_0\}$ is embedded within the total surface $\mathcal{S}=\{\mathbf{X}(\xi,\eta)\in\mathbb{R}^3|(\xi,\eta)\in\Omega\}$; as we will see in the examples of the next section, it can be the complete sphere or the cylinder of revolution, as long as the ends of the reactor coincide, see Fig. 1.

For the chemical reactor, where information on internal trajectories is not known, the total steady flux of particles, H, is

$$H=-D^*W\frac{\Delta C}{L_\xi}, \qquad (14)$$

where $\Delta C=\Delta\mathcal{C}$ is the concentration difference between the two ends of the pore and $L_\xi=\int_{\xi_0}^{\xi_f}X_\xi d\xi$ is the shortest distance along the surface. Given expression (14) as the definition of D^*, this effective diffusion coefficient measures the proportionality between the stationary flux and the difference in concentrations divided by the geodesic length along the longitudinal coordinate, L_ξ. Comparing Eqs. (13) and (14), we get:

$$\frac{1}{D^*}=\frac{W}{L_\xi}\int_0^{L_s}\frac{ds}{D_s^{\mathrm{FJ}}(s)\omega(s)\gamma(s)}. \qquad (15)$$

Since it is not always possible to analytically integrate (6) to find all quantities in terms of s, we rewrite (15) in terms of the longitudinal coordinate ξ as

$$\frac{1}{D^*}=\frac{W}{L_\xi}\int_{\xi_0}^{\xi_f}\frac{X_\xi(\xi)d\xi}{D_s^{\mathrm{FJ}}(\xi)\omega(\xi)}. \qquad (16)$$

This equation describes the effective diffusion coefficient in terms of macroscopic quantities (geometry of the reactor) and internal or local properties (such as the form of the patches or subdomains). For this reason, it is convenient to write it in terms of geometrical averages. Let us define the average of any function $f(\xi)$ along the longitudinal coordinate as $\langle f\rangle=L_\xi^{-1}\int_{\xi_0}^{\xi_f}f(\xi)X_\xi(\xi)d\xi$. This average is weighted by the metric factor that defines the arc along the longitudinal coordinate $\sigma(\xi)=\int_{\xi_0}^{\xi}X_\xi(\xi')d\xi'$.

In these terms, the reduction of the effective diffusion coefficient D^* in Eq. (15) depends on the following geometrical considerations. First, the average patch area, $A=L_\xi\langle\omega(\xi)\rangle$, i.e., the actual area covered by the paths, is less than the total area of the reactor A_{tot}; from here, we can define the ratio $\varphi=[L_\xi\langle\omega(\xi)\rangle]/A_{\text{tot}}\leqslant 1$ as a measure of surface availability (playing a similar role to porosity in the case of bulk diffusion). Second, trajectories along the surface can follow winding paths that are not necessarily geodesic. The ratio between the square lengths, one along the midline over the longitudinal coordinate (aligned with the geodesics), $\tau=(L_s/L_\xi)^2$, can be understood as a tortuosity coefficient and has the same interpretation as for bulk transport, except that in this case, we are dealing with surface trajectories. In terms of these two factors, the surface diffusion coefficient in (15), after some rearrangements, is

$$D^*=\frac{\varphi}{\tau}\left[\langle\omega(\xi)\rangle\left\langle\frac{1}{D_s^{\mathrm{FJ}}(\xi)\omega(\xi)}\right\rangle\right]^{-1}. \qquad (17)$$

In Eq. (17), we separate the transport reduction due to purely geometric factors (the coefficient φ/τ) from the contribution that depends on the local decrease in the diffusion coefficient due to confinement D_s^{FJ}, i.e., by the reduction in the flow due to the irregular shape of the patch. This term in parentheses of (17) is, therefore, a constriction factor δ and takes the form:

$$\frac{1}{\delta}=\langle\omega(\xi)\rangle\left\langle\frac{D_0}{D_s^{\mathrm{FJ}}(\xi)\omega(\xi)}\right\rangle. \qquad (18)$$

As discussed in Ref. [21], unlike the factors τ and φ, that can be measured by direct observation of the internal domains of the reactor, the constriction factor is a property of the diffusive flux. It depends on the geometry of the patch and is deduced, in our case, from the FJ approach. This way of writing the diffusion coefficient reduction in Eq. (18) is similar to that used to study the diffusion within symmetric, periodic, two-dimensional (2D) pores found in the classic references [28,29] when $X_\xi\to 1$.

In terms of these quantities, the effective diffusion coefficient from (17) is

$$D^*=D_0\frac{\varphi}{\tau}\delta, \qquad (19)$$

and can be used as an approximation in one-dimensional diffusion equations along the arc length coordinate, where the diffusion equation is

$$\omega(\sigma)\frac{\partial \hat{C}}{\partial t}(\sigma,t) \approx D^{*}\frac{\partial^2 \hat{C}}{\partial \sigma^2}. \tag{20}$$

This equation expresses the mobility reduction along transport's main direction, σ. It follows directly from the mass conservation considering that the surface flux of Fick's first law in (14) is $-D^{*}\partial\hat{C}/\partial\sigma$. Here we have written the longitudinal concentration as $\hat{C}(\sigma,t)$ to distinguish the different approaches. As we will see in our numerical examples, this coefficient D^{*} allows us to estimate and compare the MSD in different bounded domains in a straightforward way.

The normalized geodesic MSD in an elongated surface patch, where the coordinated ξ determines the long direction, can be estimated as

$$\mathrm{MSD}_{\xi} = \iint_A \sigma^2(\xi)P(\xi,t)dA \Bigg/ \iint_A P(\xi,t)dA, \tag{21}$$

where dA is the differential area and P any of the longitudinal concentrations used in this work as we will illustrate in the following study cases.

III. ILLUSTRATIVE CASES

Our study of surface diffusion has so far covered multiple spatial scales: the solution directly in the two-dimensional patch on the curved surface (Sec. II A), the one-dimensional description by projecting along the longitudinal coordinate if the patch is long enough (Sec. II B), and, finally, an average over the entire domain, knowing only the concentration at the ends of the reactor (Sec. II C). In this section, we will consider the following cases of bounded subdomains on a sphere and on a cylinder of revolution to illustrate the relevance and accuracy of our approach.

A. Patches on the sphere

Let us first consider a sphere of radius R, parameterized as $\mathbf{X} = R(\sin\theta\cos\phi, \sin\theta\sin\phi, \cos\theta)$ with (θ,ϕ) into $\Omega = [0,\pi]\times[0,2\pi)$. The parametrization is regular and the metric given by $X_\theta = R$ and $X_\phi = R\sin\theta$ depends only on θ. Therefore, in our formalism, we can consider this coordinate as the longitudinal one and identify $\xi \to \theta$ and $\eta \to \phi$. We will consider patches whose lateral edges have the form

$$\phi_j(\theta) = \phi_j^0 + a_j\cos(k_j\theta), \tag{22}$$

with $j = 1, 2$ and where parameters a_j and k_j characterize the channel shape and symmetry. We assume no flux across these boundaries. The other two boundaries (the ends of the rector) will be $\theta_i = \epsilon$ and $\theta_f = \pi - \epsilon$. According to Eq. (2), the two-dimensional concentration $C(\theta,\phi,t)$ obeys the following equation:

$$\frac{\partial C}{\partial t} = \frac{D_0}{R^2}\left[\frac{1}{\sin\theta}\frac{\partial}{\partial\theta}\left(\sin^2\theta\frac{\partial C}{\partial\theta}\right) + \frac{1}{\sin^2\theta}\frac{\partial^2 C}{\partial\phi^2}\right], \tag{23}$$

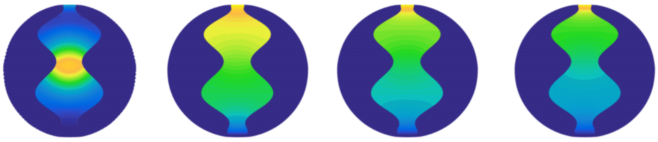

FIG. 2. Diffusion in a patch on the sphere at four different times: $t_1 = t_{\max}/240$, $t_2 = t_{\max}/10$, $t_3 = t_{\max}/4$, and $t_4 = t_{\max} = 12$. We solve Eq. (23) with zero flux boundary conditions on the large boundary and a flux crossing the domain according to $C(\theta_i) = C_{\text{in}} = 1$ and $C(\theta_f) = C_{\text{out}} = 0$. The shape of the symmetric patch uses $\epsilon = 0.2$, $\phi_1^0 = \pi/4$, $\phi_2^0 = \pi/2$, $a_1 = -1/5 = -a_2$, and $k_1 = k_2 = 2\pi$ in (22), and the parameters of the initial condition (24) are $C_n = 8.3052$, $v = 0.2$, $\theta_0 = \pi/2$, and $\phi_0 = y(\theta_0)$. The diffusion coefficient and radius of the sphere are $D_0 = 1$ and $R = 1$ and are the same for subsequent simulations.

which is solved with a pseudo-Gaussian initial condition centered on $(\theta,\phi) = (\theta_0,\phi_0)$:

$$C(\theta,\phi,t) = C_n\exp\left\{-\frac{R^2}{v^2}[(\theta-\theta_0)^2 + \sin^2\theta_0(\phi-\phi_0)^2]\right\}, \tag{24}$$

where C_n is the normalization constant and v^2 its variance. Equation (23) is solved directly on the sphere using finite-element method (FEM) simulations that we detail at the end of the section. To make this initial condition compatible with the boundary conditions, to (24) we add a Gaussian centered at θ_i of height C_i. The results are represented in Fig. 2 at four different times, where for the discretization time step we considered $\Delta t = 0.01$, and for the spatial discretization we used a triangular mesh with 10 000 elements, 5151 nodes, and $h = 5.9523\times10^{-4}$ as the maximum diameter of the elements.

These two-dimensional results are compared with those for the projected concentration obtained from the Fick-Jacobs approach. Accordingly, from Eq. (3), the marginal concentration obeys

$$R^2\sin\theta\frac{\partial c}{\partial t} = \frac{\partial}{\partial\theta}\left[D_{\text{sph}}^{\text{FJ}}w(\theta)\sin\theta\frac{\partial}{\partial\theta}\left(\frac{c}{w}\right)\right]. \tag{25}$$

To solve this equation, the values of the coefficients $w(\theta) = \phi_2(\theta) - \phi_1(\theta)$ and $y(\theta) = [\phi_1(\theta) + \phi_2(\theta)]/2$ are readily computed from (22), and the Fick-Jacobs surface diffusion coefficients in (5) is

$$D_{\text{sph}}^{\text{FJ}}(\theta) = D_0\left\{1 + \sin^2\theta\left[y'^2(\theta) + \tfrac{1}{12}w'^2(\theta)\right]\right\}^{-1}. \tag{26}$$

Equation (25) is solved for c with the initial and boundary conditions derived from those for C via the integration on Eq. (4), $c(\theta,t) = \int_{\phi_1}^{\phi_2} C(\theta,\phi,t)d\phi$. Once Eq. (25) is solved, we calculate the average concentration from Eq. (9) as $\mathcal{C} = c/w$ to compare with the two-dimensional results.

The concentration in a symmetric patch obtained from both schemes is compared in Fig. 3 (left) at four different times. The figure corroborates that the Fick-Jacobs scheme (dashed lines), based on average along the transverse direction, correctly encodes the flow reduction in the patch for the studied cases compared to the two-dimensional numerical solution (solid lines). We can indeed quantify this claim by estimating

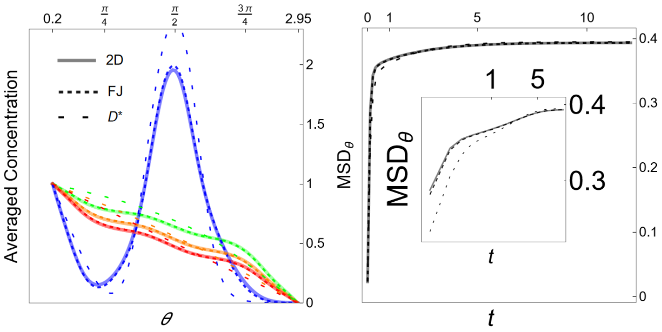

FIG. 3. Comparison of the numerical 2D solution with the FJ scheme and the effective medium approach. Left: Comparison between the averaged concentration derived from the direct solution of the 2D problem in Eq. (23) (solid line), the obtained from the FJ procedure by solving (25) and computing c/w (dashed line), and that of the effective medium approach by solving Eq. (31) (dotted line). The same four times of Fig. 2 are shown in blue, green, orange, and red, respectively. Right: Geodesic MSD derived from the three approaches using Eq. (32). Inset: MSD at short times showing a small slope preceding the plateau.

the major relative error between the FJ solution and the FEM one, computed with L_∞ norm. The largest percentage error is 6.5% at short times ($t = 0.05$) and decreases as the system evolve to 0.7% at t_{max}. These numerical results are significant as they confirm the adequacy of our hypothesis $C \approx \mathcal{C}$, used to estimate the macroscopic flow.

In the last stage, we average the resistance to flow in the longitudinal direction along the midline of the patch. For the sphere, the coordinate describing the length along this coordinate, from Eq. (6), is

$$s(\theta) = R\int_{\theta_i}^{\theta} d\theta'\sqrt{1+\sin^2(\theta')y'^2(\theta')}, \tag{27}$$

which reduces to $s(\theta) = R(\theta - \theta_i)$ for symmetric patches, i.e., the geodesic distance along parallels. The width of the pore is $\omega(\theta) = R\sin(\theta)w(\theta)$, which is the geodesic distance along meridians.

The available area ratio φ is

$$\varphi = \frac{1}{WL}\int_{\theta_i}^{\theta_f} R^2\sin(\theta)w(\theta)d\theta = \frac{1}{A_{\text{tot}}}\left[\int_{\theta_i}^{\theta_f}\int_{\phi_1(\theta)}^{\phi_2(\theta)} dA\right], \tag{28}$$

where $dA = R^2\sin(\theta)d\theta d\phi$ is the differential of surface area. In this equation, it is clear that φ represents the ratio among the patch area (the term inside square brackets) and the total area of the spherical reactor $A_{\text{tot}} = WL_\theta$. The tortuosity coefficient is

$$\tau = \left[\frac{s(\theta_f)}{L_\theta}\right]^2 = \left[\frac{1}{\theta_f-\theta_i}\int_{\theta_i}^{\theta_f} d\theta'\sqrt{1+\sin^2(\theta')y'^2(\theta')}\right]^2, \tag{29}$$

which represents how the trajectories deviate from the parallels, with minimum geodesic distance between ends $L_\theta = R(\theta_f - \theta_i)$. The constriction factor δ from Eq. (18) is given by

$$\frac{1}{\delta} = \frac{1}{(\theta_f-\theta_i)^2}\int_{\theta_i}^{\theta_f}\sin(\theta)w(\theta)d\theta\cdot\int_{\theta_i}^{\theta_f}\frac{D_0\,d\theta}{D_{\text{sph}}^{\text{FJ}}(\theta)\sin\theta\, w(\theta)}. \tag{30}$$

From the three previous expressions, it is possible to obtain the effective diffusion coefficient in (19). By this means, the diffusion equation in the sphere along the longitudinal coordinate $\sigma = R\theta$ is approximated by Eq. (20) as follows:

$$\sin(\theta)w(\theta)\frac{\partial\hat{C}}{\partial t}(\theta,t) \approx \frac{D^*}{R^2}\frac{\partial^2\hat{C}}{\partial\theta^2}, \tag{31}$$

and can be solved in the domain $\sigma \in [0, L_\theta]$ with the same initial and boundary conditions used for $\mathcal{C}$. The results are plotted in Fig. 3 (dotted line in the left panel) and compared with the two-dimensional solution (solid line) and the FJ scheme (dashed line) for the symmetric channel. As can be seen, the Eq. (31) closely reproduces the results of the numerical simulations for the mean concentration. For the nonstationary case, this equation contains the minimum shape and curvature factors for the description in the term $\sin(\theta)w(\theta)$. More importantly, for large reactors in the steady state, it establishes that the average flux in the reactor is $-D^*\Delta C/\Delta s$, where the effective diffusion coefficient only depends on averaged quantities: constriction, tortuosity, and available surface factors.

Figure 4 shows three channels on the sphere with different averaged properties. The diffusion coefficients $D_{\text{sph}}^{\text{FJ}}$ are different in each case. Moreover, although qualitatively, the concentrations and MSD are similar for each channel, slight differences in their evolution toward the steady state for different values of the tortuosity, constriction, and available area can be appreciated. However, when calculating the relative percentage errors for long times, the tortuous channel has the highest error of around 3%, and the straight channel has the slightest error of around 0.01%, indicating an excellent estimation.

As shown in this section, our approach allows us to estimate approximate solutions for the average concentration under different detail degrees. In all the cases, the concentration along the longitudinal direction is approximately the same, and the normalized geodesic MSD in (21) for the sphere is expected to be the same:

$$\text{MSD}_\theta(t) = \int_{\theta_i}^{\theta_f}(R\theta)^2 P\sin(\theta)w\,d\theta \Bigg/ \int_{\theta_i}^{\theta_f} P\sin(\theta)w\,d\theta. \tag{32}$$

In this equation, the concentration can be deduced from any of our approaches by choosing $P = \{\mathcal{C}, c/w, \hat{C}\}$. To test this idea, in Fig. 3 (right), we compare the results for the MSD when using (1) the two-dimensional simulations for C in (23) and (9), (2) the Fick-Jacobs approach for c/w with (25), and (3) the macroscopic equation for $\hat{C}$ in (31), showing a general concordance of the geodesic MSD in all cases. Remarkably, the behavior of the FJ projection and the full solution are very comparable, and although the averaged approximation deviates a bit at short times, for longer times it also reaches the plateau. However, from the three approaches something interesting can be seen, namely there is a transient regime

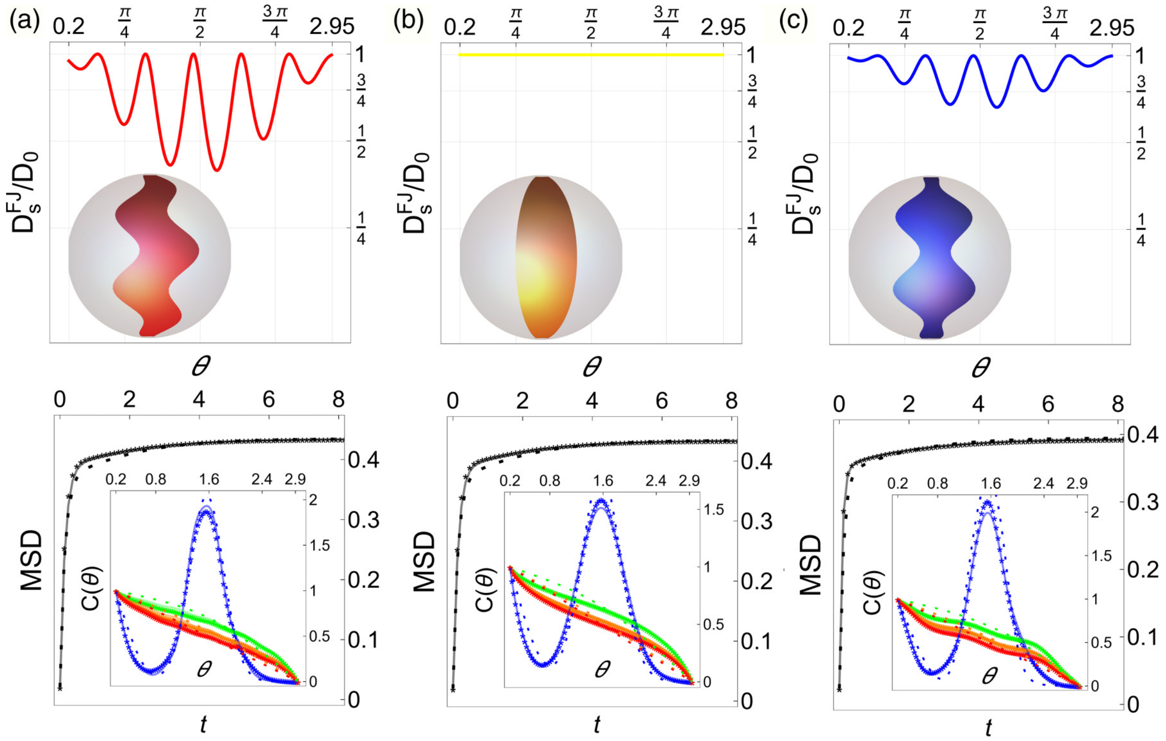

FIG. 4. Diffusion and MSD for three different patches on the sphere. Upper row: We plot the FJ diffusion coefficient and each patch on the sphere in the inset. On the left is an asymmetrical channel, in the center a straight symmetrical channel, and on the right a symmetrical channel with periodical boundaries. Parameters of Eq. (22) are the same that for Fig. 2 in last plot, and we change to $a_2 = a_1 = 1/5$, $h = 4.3079 \times 10^4$ in the first plot and (c) $a_1 = a_2 = 0$, $h = 4.3063 \times 10^4$ for the central figure. Lower row: We plot the longitudinal MSD defined in Eq. (32) for each patch using two-dimensional simulations (solid line), FJ approach (dashed line) and effective model (dotted line). In the inset we plot the averaged concentration for four different times. All other parameters of these simulations are the same as in Fig. 3.

just before the beginning of the plateau that can be fitted to a straight line with a reduced but nonzero slope. This is precisely the kind of behavior exhibited at long times for very long narrow channels with the Fick-Jacobs projection.

B. Patches on cylinders

The sphere provides a simple archetypical system for testing our ideas and applies primarily to closed membrane surfaces. However, transport in most reactors of practical interest occurs along interstitial pathways along a cylinder, as in zeolites.

Let us now consider the surface of a cylinder of variable radius $R(z)$ parameterized as $\mathbf{X} = (R(z)\cos\phi,\ R(z)\sin\phi,\ z)$. The entire surface of revolution is given by $(z, \phi) \in \Omega = [0, L] \times [0, 2\pi]$, where L is the height of the cylinder. The parametrization is regular and is defined by the factors $X_z = \sqrt{1 + R'^2(z)}$ and $X_\phi = R(z)$ that depend only on the vertical coordinate z. Therefore, we can consider in our formalism $\xi \to z$, and $\eta \to \phi$. This implies that the longitudinal paths can be taken along z with the long edges defined as in (22) for the angular coordinate. The top and bottom borders are defined by $z_i = 0$ and $z_f = L$. In this geometry, the local surface diffusion coefficient in Eq. (5) is as follows:

$$D^{\rm FJ}_{\rm cyl}(z) = D_0\left\{1 + \left[\frac{R^2(z)}{1 + R'^2(z)}\right]\left[y'^2(z) + \frac{1}{12}w'^2(z)\right]\right\}. \tag{33}$$

The complete derivation to obtain all the diffusion equations and the different geometric factors to determine the diffusion in a patch in a cylinder are done similarly as for the sphere and therefore are omitted from this presentation. We simply establish that the geodesic MSD measured along the vertical in a cylinder, from Eq. (21), is given by

$$\mathrm{MSD}_z = \iint_A \sigma^2(z)P(z,t)dA \Big/ \iint_A P(z,t)dA, \tag{34}$$

where we have used that the longitudinal arc length is

$$\sigma(z) = \int_0^z \sqrt{1 + R'^2(\hat{z})}d\hat{z}, \tag{35}$$

and the differential area of the cylinder is $dA = R(z)\sqrt{1 + R'^2}dzd\phi = R(z)w(z)\sqrt{1 + R'^2}dz$.

Figure 5 shows our simulations' results for three different patches; to get those results we used $\Delta t = 0.01$ for the time, and for the spatial discretization, as in the sphere case, we used a triangular mesh with 10 000 elements, 5151 nodes, but with $h = 0.0018$ for channels (a) and (b) and $h = 0.0027$ for the case (c). As we can see, there is general agreement in all cases for the spatiotemporal concentration profiles and the geodesic MSD. The approximation for the effective medium scheme is even better than for spheres since the patches in a cylinder are larger, improving the approximation. In this case, the relative error for FJ at large times was 4% for the tortuous channel and 0.02% for the straight one, yielding excellent results again.

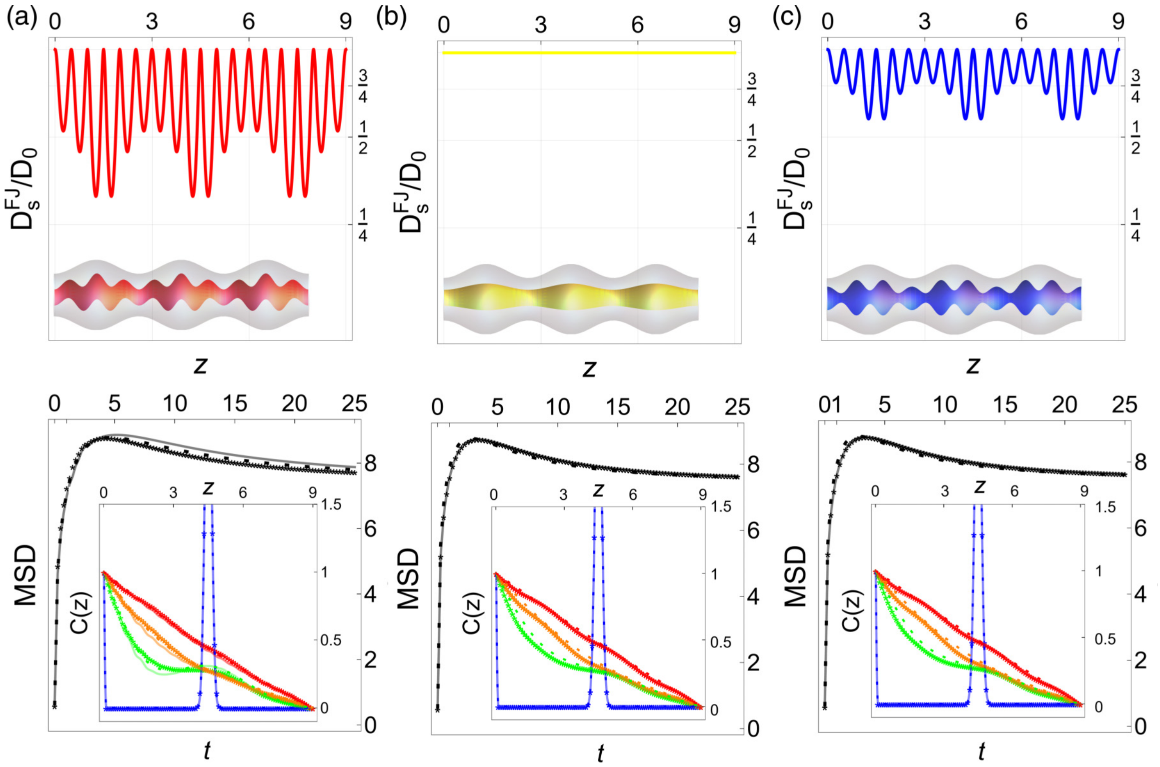

FIG. 5. Diffusion over three patches on a cylinder. The upper row shows the FJ diffusion coefficient in each case and the corresponding patch on the cylinder surface. Patch pathways generated by Eq. (22) using (a) $a_1 = -a_2 = 1/5$, (b) $a_1 = a_2 = 1/5$, and (c) $a_1 = a_2 = 0$. In all cases, we take $k_1 = k_2 = \pi$, $\phi_1^0 = \pi/2$ and $\phi_1^0 = 3\pi/2$, $D_0 = 1$, and $t_{\max} = 25$. The variable radius of the cylinder is $R(z) = 1 - (1/4)\cos(6\pi z/L)$ where $L = 9$.

Finally, we use the backward Euler scheme for the discretization in time and a linear Lagrangian finite-element method for the solution of the Laplace-Beltrami operator in space, to obtain the numerical solution. This approximation is obtained directly by employing Cartesian coordinates instead of the given parametrization. From a numerical and computational point of view, it is convenient to discretize the Laplace-Beltrami operator after projecting the gradient to the corresponding target direction on the surface. Also, this is done as the corresponding discretization of the Laplace-Beltrami operator yields a discrete time-dependent linear system (first-order linear ordinary differential equation). This approach is also very convenient when there is no explicit parametrization of the surface. For the details about this implementation we refer to Ref. [41].

IV. SUMMARY AND DISCUSSION

In this work, we present a proposal to study diffusion in finite subdomains on curved surfaces. This proposal is motivated by the need for an adequate definition of the diffusion coefficient that can be experimentally measured for surface diffusion in chemical reactors, where the individual trajectories are not of interest but quantities reflecting the average flow rate. Since the space available in the reactor is narrow due to the confined trajectories of the adsorbed particles, it is possible to use entropic and reduction arguments to find two different coefficients that reflect different averages. First, we compute a position-dependent diffusion coefficient, the so-called Fick-Jacobs coefficient, which contains information about the surface's variations and the boundary's internal geometry. Then, from this one, it was possible to obtain an effective diffusion coefficient D^* in terms of quantities commonly used in the description of pores, such as concavity, tortuosity, and degree of constriction [47]. The main result of this paper is precisely this effective diffusion coefficient that considers the curvature of the surface, the shape of the physical boundaries that restrict motion, and the way the diffusive flux averages through constrictions and tortuosities of narrow paths over the main transport direction. This coefficient allows using a 1D diffusion equation along an effective longitudinal coordinate, whose solution closely approximates the numerically calculated surface diffusion with constrictions. Indeed, when calculating the relative percentage errors at long times, it was found that the highest value occurs in tortuous channels and the smallest in straight ones, ranging from 4.0% to 0.01% on both surfaces. Remarkably, the coefficient in Eq. (17) has a similar form to the effective diffusion coefficient obtained by Lifson-Jackson [28], and Festa-d'Agliano [29] and reduces to it for symmetric patches on flat surfaces. However, our deduction is more general and does not require the periodicity constraint on the channel walls as in those traditional schemes.

We have also shown that the Fick-Jacobs scheme and the effective mean approach allow us to predict the geodesic MSD successfully. It is known, from Brownian dynamics simulations [48,49], that the mean-square angular displace-

TABLE I. Summary of the data of the geometric coefficients involved in the reduction of the diffusion coefficient for the patches studied in this work.

Sphere						Cylinder					
Fig.		Coefficients			Diffusion	Fig.		Coefficients			Diffusion
4	Patch	ϕ	δ	τ	D^*/D_0	5	Patch	ϕ	δ	τ	D^*/D_0
a		0.125	0.622	1.42	0.0547	a	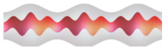	0.125	0.578	1.669	0.0433
b		0.125	0.833	1	0.1042	b	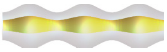	0.125	0.939	1	0.1211
c		0.122	0.642	1	0.0787	c	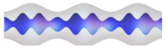	0.125	0.688	1	0.0862

ment for free diffusion over the whole sphere starts linearly in time, like free diffusion in the plane, then has a transient and finally has a plateau for long times. Similar behavior for the MSD, for both short and long times, is observed in our simulations. However, in our case, just before the plateau, a region with a nonzero slope but less than the initial one appears. This behavior is similar to a narrow channel and indicates an exploration process of the particles within the confinement, [44,45,50].

It is worth stressing that, given the averaged nature of this coefficient, its relation to the system squared length provides a characteristic rate of the surface diffusion process that differs for each patch shape, as shown in Table I, where the diffusion coefficients for the tortuosity, constriction, and available area values of the examples studied in this work are presented. Therefore, for systems involving adsorption, heterogeneous catalysis, or bulk diffusion, this D^* coefficient allows comparison with the rates of the other processes and, consequently, measures the actual influence of surface diffusion in each reactor [6]. The relevance of the effective diffusion coefficient in finding the concentration profiles and the MSD is not restricted to constant external flux conditions, such as those used in this work. As demonstrated in both Ref. [21] for flat surfaces and in our numerical experiments for curved domains, the D^* coefficient is also suitable for periodic or zero-flux conditions as long as the patch is large enough. As argued in Ref. [21], this is because the flow resistance was derived for infinitesimal intervals. Therefore, the approximation is valid even for slight concentration differences, which makes the approach valid for both equilibrium and nonequilibrium conditions.

We also observe that, as for flat surfaces, the diffusion coefficient of the Fick-Jacobs approximation used in this work in Eq. (5) can be improved. To do so, higher-order terms in the width-to-length aspect ratio must be included in the expansion for D_s^{FJ}, possibly by improving the fits to the data [37]. However, these improvements do not affect the theory we have constructed for D^* and should be considered in future works.

A potential application of the findings obtained in this study is to directly quantify mass transport in various experiments where surface diffusion is recorded through an effective diffusion coefficient that implicitly accounts for surface shape, and size [51,52]. Moreover, as already done for planar surfaces [53–55], the model can be immediately generalized to consider ionic transport, also present in experiments and models of electrodiffusion in confined curved domains.

Additionally, the surface diffusion process is intrinsically linked to adsorption. For more general scenarios, when bulk dynamics is considered, even anomalous behavior can be obtained for surface motion [56]. However, as we said before, in our approximation, the role of the surface is only to restrict the trajectories to a diffusive movement in the space defined by it, which means that the particles are already adsorbed on the surface and that the strength of this binding is mainly reflected in their surface diffusion coefficient, D_s. This coefficient determines the kind of adsorption between the particle and surface through its motility in the mean-field approximation. As a result, we have been able to find the ratio between the coefficient measured on an irregular surface D^* and that of a flat surface D_{s0}. However, future work will allow us to incorporate surface diffusion with other processes, such as those occurring in heterogeneous catalysis involving surface adsorption or desorption [57]. For this purpose, the availability and chemical affinity between adsorbed particles with concentration C_s and bulk particles with concentration C_b are coupled, following Refs. [16,17]. Then, it was shown that the decrease in the surface diffusion coefficient due to the kind of adsorption could be quantified through the parameter $\lambda = \partial C_s/\partial C_b$ that measures the exchange rate between bulk and surface particles. In first approximation, the reduction is given by $D_s\frac{\lambda}{1+\lambda}$, which means that if the adsorption is weak ($\lambda \to 0$), the effective superficial diffusion coefficient tends to zero since there are no adsorbed particles. On the other hand, if the adsorption is efficient ($\lambda \geqslant 1$), then the effective diffusion increases to a saturation value D_s, limited since the available slots for adsorption on the surface are finite.

Further extensions may be considered. For instance, particle motion is usually driven by an external potential producing a force along the channel's axis in channel transport processes. In this case, the free energy contains the external and entropic potentials, so the average particle current explicitly contains the external force. Indeed, the ratio between the average particle current and the applied force, known as nonlinear mobility, is one of the fundamental quantities in these systems [58,59]. For periodic potentials and channels, the mobility depends on the longitudinal variable, the ratio between the potential energy and the thermal energy, and the shape of the channel through the position-dependent diffusion coefficient [58,59]. For the systems studied in this paper involving tortuous channels on curved surfaces, the mobility will be modified to consider beyond periodic boundaries when using our approach, similar to what happens with the Lifson-Jackson coefficient. This calculation will be discussed elsewhere.

Accordingly, the present study's results, especially the effective diffusion coefficient D^*, provide a valuable tool for studying surface diffusion in tortuous and curved domains.

ACKNOWLEDGMENTS

We thank DCBI of UAM-Iztapalpa for financial support under the Programa Especial de Apoyo a Proyectos de Docencia e Investigación 2021 and PRODEP program for the grant UAM-PTC-710. G.C.-A. also acknowledges support form the grant Becas de Superación Académica Elisa Acuña 2021 from Universidad Autónoma Metropolitana.

---

[1] A. Kapoor, R. Yang, and C. Wong, Catal. Rev. **31**, 129 (1989).
[2] J. H. Koh, P. C. Wankat, and N. H. L. Wang, Ind. Eng. Chem. Res. **37**, 228 (1998).
[3] M. Y. Sengul, J. Guo, C. A. Randall, and A. C. van Duin, Angew. Chem. **131**, 12550 (2019).
[4] L. Roybal and S. Sandler, AIChE J. **18**, 39 (1972).
[5] G. Allaire and H. Hutridurga, IMA J. Appl. Math. **77**, 788 (2012).
[6] I. Medveď and R. Černý, Micropor. Mesopor. Mat. **142**, 405 (2011).
[7] S. Sircar and M. Rao, AIChE J. **36**, 1249 (1990).
[8] D. Weber, A. J. Sederman, M. D. Mantle, J. Mitchell, and L. F. Gladden, Phys. Chem. Chem. Phys. **12**, 2619 (2010).
[9] G. Antczak and G. Ehrlich, Surf. Sci. Rep. **62**, 39 (2007).
[10] W. Ren, G. Li, S. Tian, M. Sheng, and L. Geng, Ind. Eng. Chem. Res. **56**, 3446 (2017).
[11] G. L. Kellogg, Surf. Sci. Rep. **21**, 1 (1994).
[12] J. G. Choi, D. D. Do, and H. D. Do, Ind. Eng. Chem. Res. **40**, 4005 (2001).
[13] P. Schneider and J. Smith, AIChE J. **14**, 886 (1968).
[14] S. Rutherford and D. Do, Adsorption **3**, 283 (1997).
[15] S. T. Hwang and K. Kammermeyer, Can. J. Chem. Eng. **44**, 82 (1966).
[16] A. Ledesma-Durán, S. Hernández, and I. Santamaría-Holek, J. Phys. Chem. C **121**, 14544 (2017).
[17] A. Ledesma-Durán, S. Hernández, and I. Santamaría-Holek, J. Phys. Chem. C **121**, 14557 (2017).
[18] G. Rhead, Surf. Sci. **47**, 207 (1975).
[19] H. Tamon, M. Okazaki, and R. Toei, AIChE J. **31**, 1226 (1985).
[20] J. A. Ochoa-Tapia, J. A. Del Rio P, and S. Whitaker, Chem. Eng. Sci. **48**, 2061 (1993).
[21] A. Ledesma-Durán, S. I. Hernández, and I. Santamaría-Holek, Phys. Rev. E **95**, 052804 (2017).
[22] Z. Sun, X. Tang, and G. Cheng, Micropor. Mesopor. Mat. **173**, 37 (2013).
[23] D. Mu, Z. S. Liu, C. Huang, and N. Djilali, Microfluid. Nanofluid. **4**, 257 (2008).
[24] D. Mu, Z. S. Liu, C. Huang, and N. Djilali, J. Porous Mater. **14**, 49 (2007).
[25] M. Wang, Y. Hou, L. Yu, and X. Hou, Nano Lett. **20**, 6937 (2020).
[26] R. Varma and S. Mayor, Nature (Lond.) **394**, 798 (1998).
[27] C. J. Thompson, D. F. Kienle, and D. K. Schwartz, J. Phys. Chem. Lett. **13**, 2901 (2022).
[28] S. Lifson and J. L. Jackson, J. Chem. Phys. **36**, 2410 (1962).
[29] R. Festa R and E. Galleani d'Agliano, Phys. A **90**, 229 (1978).
[30] G. Chacón-Acosta, I. Pineda, and L. Dagdug, J. Chem. Phys. **139**, 214115 (2013).
[31] I. Pineda, G. Chacón-Acosta, and L. Dagdug, Eur. Phys. J.: Spec. Top. **223**, 3045 (2014).
[32] R. Zwanzig, J. Phys. Chem. **96**, 3926 (1992).
[33] D. Reguera and J. M. Rubi, Phys. Rev. E **64**, 061106 (2001).
[34] P. Kalinay and J. K. Percus, J. Chem. Phys. **122**, 204701 (2005).
[35] P. Kalinay and J. K. Percus, Phys. Rev. E **74**, 041203 (2006).
[36] R. M. Bradley, Phys. Rev. E **80**, 061142 (2009).
[37] L. Dagdug and I. Pineda, J. Chem. Phys. **137**, 024107 (2012).
[38] L. Dagdug, A. García-Chung, and G. Chacón-Acosta, J. Chem. Phys. **145**, 074105 (2016).
[39] Y. Chávez, G. Chacón-Acosta, and L. Dagdug, J. Phys.: Condens. Matter **30**, 194001 (2018).
[40] Y. Chávez, G. Chacón-Acosta, and L. Dagdug, J. Chem. Phys. **148**, 214106 (2018).
[41] D. A. León Velasco, R. Glowinski, and L. H. Juárez-Valencia, ESAIM Contr. Optim. Calc. Var. **22**, 1054 (2016).
[42] R. G. Plaza, F. Sanchez-Garduño, P. Padilla, R. A. Barrio, and P. K. Maini, J. Dyn. Differ. Equ. **16**, 1093 (2004).
[43] P. S. Burada, P. Hänggi, F. Marchesoni, G. Schmid, and P. Talkner, ChemPhysChem **10**, 45 (2009).
[44] L. Dagdug, M. V. Vazquez, A. M. Berezhkovskii, and S. M. Bezrukov, J. Chem. Phys. **133**, 034707 (2010).
[45] A. M. Berezhkovskii, L. Dagdug, and S. M. Bezrukov, J. Chem. Phys. **143**, 164102 (2015).
[46] J. Faraudo, J. Chem. Phys. **116**, 5831 (2002).
[47] C. F. Berg, Transp. Porous Media **103**, 381 (2014).
[48] P. Castro-Villarreal, A. Villada-Balbuena, J. M. Méndez-Alcaraz, R. Castañeda-Priego, and S. Estrada-Jiménez, J. Chem. Phys. **140**, 214115 (2014).
[49] A. Valdés Gómez and F. J. Sevilla, J. Stat. Mech. (2021) 083210.
[50] A. Ledesma-Durán, J. Munguía-Valadez, J. A. Moreno-Razo, S. Hernández, and I. Santamaría-Holek, Front. Phys. **9**, 634792 (2021).
[51] T. Titze, A. Lauerer, L. Heinke, C. Chmelik, N. E. R. Zimmermann, F. J. Keil, D. M. Ruthven, and J. Kärger, Angew. Chem. Int. Ed. **54**, 14580 (2015).
[52] J. Kärger and R. Valiullin, Chem. Soc. Rev. **42**, 4172 (2013).
[53] I. Santamaría-Holek, A. Ledesma-Durán, S. I. Hernández, C. García-Alcántara, A. Andrio, and V. Compañ, Phys. Chem. Chem. Phys. **22**, 437 (2020).
[54] U. M. B. Marconi, S. Melchionna, and I. Pagonabarraga, J. Chem. Phys. **138**, 244107 (2013).
[55] A. Fuliński, I. Kosińska, and Z. Siwy, New J. Phys. **7**, 132 (2005).

[56] A. V. Chechkin, I. M. Zaid, M. A. Lomholt, I. M. Sokolov, and R. Metzler, Phys. Rev. E **86**, 041101 (2012).

[57] I. Santamaría-Holek, S. I. Hernández, C. García-Alcántara, and A. Ledesma-Durán, Catalysts **9**, 281 (2019).

[58] D. Reguera, G. Schmid, P. S. Burada, J. M. Rubí, P. Reimann, and P. Hänggi, Phys. Rev. Lett. **96**, 130603 (2006).

[59] P. S. Burada, G. Schmid, D. Reguera, J. M. Rubí, and P. Hänggi, Phys. Rev. E **75**, 051111 (2007).